

基于 OCDR 的飞秒激光直写光波导微结构在线监测

夏龙^{1,2}, 王新悦^{1,2}, 吴胜保^{1,2*}, 崔省伟^{1,2}, 冯亭^{1,2}, 姚晓天^{1,2}¹河北大学物理科学与技术学院光信息技术创新中心, 河北 保定 071002;²河北省光学感知技术创新中心, 河北 保定 071002

摘要 飞秒激光直写技术具有无掩模、真三维、高精度等优点,在透明介质光波导器件立体加工中具有很好的应用前景。然而,实际加工中需根据目标材料的特性反复探索和优化加工参数,过程繁琐且复杂。提出了一种基于光相干域反射仪(OCDR)在线监测飞秒激光在已有波导中直写加工微结构或器件的新技术,以光纤波导为例研究了激光脉冲能量、脉冲频率及直写速率对加工结构回波反射特性的影响,并分析了反射特性与加工工艺参数的对应关系。研究表明:通过 OCDR 反射曲线突变点能够快速准确地确定引起材料性质改变的激光能量和脉冲频率的阈值条件,且根据曲线变化趋势和反射峰特点可判断材料性质改变类型;此外,通过分布式测量激光直写反射曲线,可获得加工速率对加工效果的影响规律。该技术为波导内飞秒激光直写微结构或器件工艺参数的摸索提供了一种非破坏、高效、在线的解决方案。

关键词 激光技术; 飞秒激光; 光波导; 微纳加工; 分布式光纤传感; 反射特性

中图分类号 TN249; TN252 **文献标志码** A

DOI: 10.3788/CJL221411

1 引言

自 1996 年第一次被证实能够在透明介质内部诱导折射率改变^[1]以来,飞秒激光直写技术以其真三维、无掩模、加工灵活等独特的优势,被广泛应用于光纤光栅^[2-7]、光纤微结构^[8-13]、光子芯片^[14-19]等透明介质波导器件的加工中。尽管目前已有大量关于飞秒激光对透明介质材料折射率修饰的研究报道^[20-24],但仍没有成熟理论模型能够完全描述其对介质材料折射率的作用机理。在实际加工中,为了获得较好的加工效果,往往需要根据目标材料的特性进行大量实验研究,反复探索和优化激光加工参数,过程繁琐且复杂。

目前,飞秒激光直写工艺参数的研究通常采用电子扫描显微镜和原子力显微镜进行后处理验证^[25-30],尽管这种方法可提供大量基于处理结构的高分辨率图像优化参数集的信息,但无法呈现加工的动态过程及瞬态,这意味着每一个流程都需要稳定且可重复,因此需要大量的时间和生产成本。此外,将飞秒激光加工系统与高分辨光学显微镜相结合以获取激光加工微结构图像的方法也已被广泛应用到波导器件加工中^[17,31-34],此方法可对加工参数进行适当的实时反馈控制,在没有最佳加工参数的情况下,可对未知材料进行加工,且能直接观察加工后的结构。然而,使用光学显

微镜进行过程监测时,目标样品仅限于对照明光透明的材料,且仅限于在样品表面附近加工,以防止样品受衍射影响。最近,一些基于相干成像的在线的监测手段被用于飞秒激光加工效果的测量表征^[35-39],这些技术不仅可获得加工结构的二维平面形貌,还能获得加工深度信息。然而这些手段对背向散射信号的测量动态范围有限,尽管可用于表征破坏性的微纳加工,但对飞秒激光波导器件加工中材料改性产生的折射率改变引起的微弱散射信号的测量能力不足。

为快速获得飞秒激光直写光波导器件的工艺参数及加工效果,本文提出了一种基于光相干域反射仪(OCDR)在已有波导中确定飞秒激光直写加工微结构的分布式、在线监测技术。不同于已有的飞秒激光加工工艺监测手段,本文利用 OCDR 系统的高回波损耗测量精度和大动态范围,通过加工波导器件过程中的背向反射信号变化实现工艺参数的监测。以飞秒激光直写光纤微结构为实验对象,研究了激光脉冲能量、脉冲频率及直写速率三个关键工艺参数对光纤反射特性的影响,建立了 OCDR 测量的反射特征曲线与加工工艺参数的对应关系模型。通过该模型能够快速准确地确定引起材料性质改变的激光能量和脉冲频率的阈值条件,且根据曲线变化趋势和反射曲线特点可判断材料性质改变的类型。此外,利用 OCDR 的分布式、在

收稿日期: 2022-11-14; 修回日期: 2022-12-08; 录用日期: 2023-01-03; 网络首发日期: 2023-01-12

基金项目: 国家自然科学基金(12004092, 61975049)、河北省重点研发计划(19212109D, 20542201D)、河北省高等学校科学技术研究项目(QN2020259)、河北大学高层次人才科研启动经费(521000981006, 521000981203)

通信作者: *swu@hbu.edu.cn

线监测能力,还获得了直写速率对加工效果的影响规律。

2 实验装置及原理

2.1 OCDR 系统原理

光相干域反射仪系统原理图如图 1 所示。该系统由经典的白光迈克耳孙干涉仪发展而来^[40-41],超辐射发光二极管(SLD)发出的宽带光信号经过耦合器 1 (分光比为 90:10)后分为参考路光和待测路光。待测

路中的可调延迟线用于调节光程差,实现波导传输方向不同位置反射信号的扫描测量,延迟线最大扫描范围为 60 cm,扫描一次时间为 20 s,实际测量中可以根据待测区域长度调整扫描范围,缩短扫描时间。开启实时扫描后,在设定范围内进行自动重复扫描,参考光与待测样品不同位置的后向瑞利散射光在耦合器 2 (分光比为 50:50)中发生干涉,通过双平衡探测器抑制共模噪声,干涉信号转化为电信号,利用信号处理器获得样品不同位置的离散反射谱。

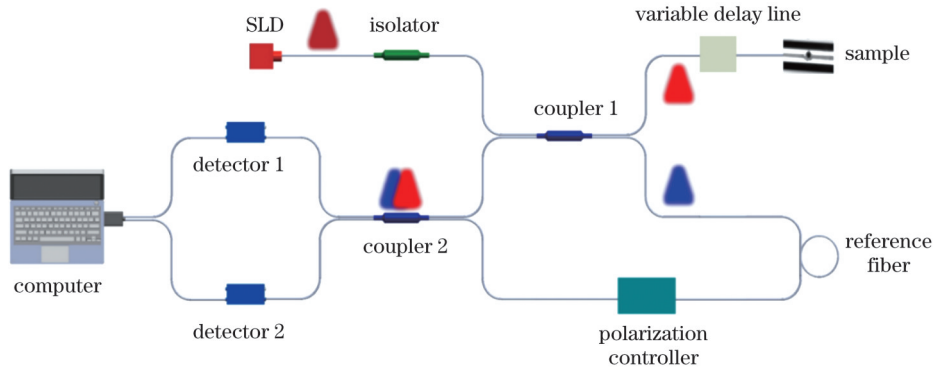


图 1 OCDR 系统原理图

Fig. 1 Schematic of OCDR system

分别使用 $E_s(t, L_s)$ 和 $E_r(t, L_r)$ 表示光相干域反射仪样品路和参考路的光场, L_s 和 L_r 分别为样品路和参考路的光程。假设探测器能够捕获所有从参考路和样品路返回的光,则探测到的干涉光强^[42]可表示为

$$I(t) = |E_s(t, 2L_s)|^2 + |E_r(t, 2L_r)|^2 + 2\text{Re}[E_r(t, 2L_r)E_s^*(t, 2L_s)], \quad (1)$$

式中: $\text{Re}[\cdot]$ 表示取实部; $*$ 表示取共轭。

发生干涉的两列光波必须满足光程差在光源的相干长度内,假设 SLD 光源输出的是理想的高斯光谱,且不考虑系统色散的影响,系统理论分辨率 (Δl) ^[39]可根据光源光谱的傅里叶变换计算得到:

$$\Delta l = \frac{2 \ln 2}{\pi} \cdot \frac{\lambda_c^2}{n \Delta \lambda}, \quad (2)$$

式中: λ_c 为光源的中心波长; $\Delta \lambda$ 为光谱的半峰全宽

(FWHM); n 为被测单元的有效折射率。由式(2)可知,采用宽带光源可有效提升 OCDR 的分辨率性能。为降低色散对分辨率的影响,本系统采用中心波长在 1310 nm 附近、FWHM 为 40 nm 的 SLD 光源,由式(2)可得系统理论分辨率约为 13 μm 。此外,系统的关键性能指标还包括回波测量动态范围(-10 dB ~ -95 dB)、回波测量精度(± 1.0 dB)、长度测量范围(60 cm, 空气中)、定位精度(0.1 mm)。

图 2(a)所示为光谱仪实测的 SLD 光源的功率谱密度。可以看出,实测光谱呈高斯分布,其峰值波长为 1300 nm, FWHM 为 39.2 nm, 与理论值非常接近。图 2(b)为该系测量的飞秒激光直写光纤中相距 13.5 μm 的两个缺陷点的反射曲线,飞秒激光脉冲能量为 0.355 μJ , 脉冲频率为 1 kHz。其中虚线为写入第一

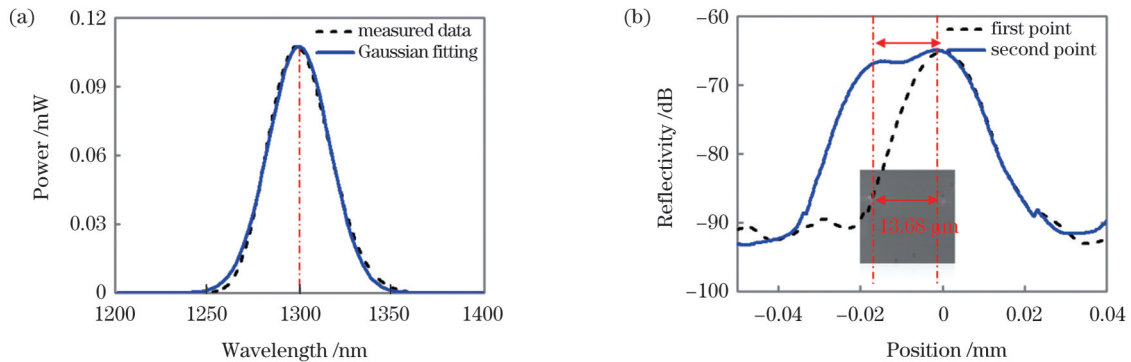


图 2 OCDR 性能验证。(a) SLD 光源光谱; (b) OCDR 测量的光纤中两个缺陷点反射曲线

Fig. 2 OCDR performance verification. (a) Spectrum of SLD source; (b) reflection curves of two defect points in optical fiber measured by OCDR

个点时测得,实线为写入两个点时测得。通过图 2 中两个反射峰峰值位置计算得到实测距离为 $13.68 \mu\text{m}$,很好地验证了系统分辨率和位置测量精度。此外,可以看出,该系统可监测的最小回波损耗约为 -95 dB 。

2.2 实验装置

OCDR 在线监测飞秒激光直写加工实验装置如图 3 所示。该装置主要由飞秒激光系统、高精度三维位移平台、显微镜观测系统、光纤夹具、OCDR 系统等部分组成。飞秒激光系统发射的激光脉冲(中心波长为 1030 nm ,脉冲持续时间为 382 fs)先通过由半波片(HWP)和偏振分束器(PBS)组成的脉冲能量控制器,再经透镜和反射镜进入扩束系统进行光斑整形,最后

被油浸物镜(数值孔径为 $NA=1.32$,放大倍数为 $60\times$)聚焦后进入激光加工位移台。待加工光纤被光纤夹具固定在位移平台,光纤中的一端与 OCDR 系统连接,通过与位移台关联的显微镜观测系统,可实时观察垂直方向焦点及光纤的相对位置,进而确定直写加工位置。在飞秒激光加工过程中,通过实时开启 OCDR 进行扫描测量,即可获得光纤内部不同位置的反射信号。利用该技术也可在其他波导中进行器件加工或结构修饰监测,近期本课题组已利用 OCDR 实现了光芯片内部器件结构的识别及缺陷的探测和定位^[41]。如果把芯片与光纤耦合封装后置于加工平台上,则完全可实现片上波导的飞秒激光直写加工的在线监测。

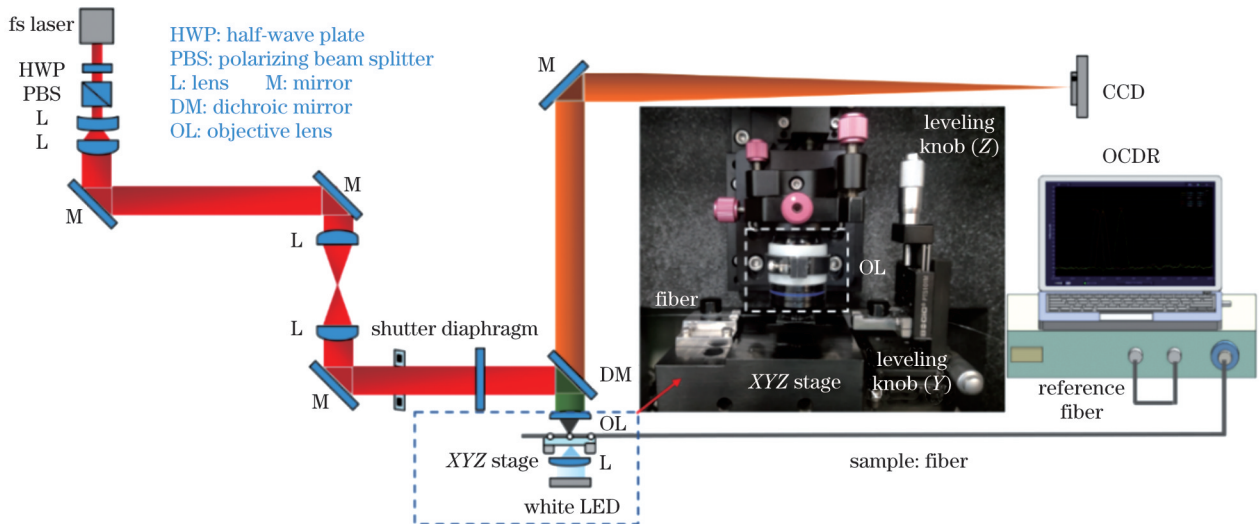


图 3 OCDR 系统在线监测的飞秒激光光纤微加工实验装置图

Fig. 3 Femtosecond laser fiber micromachining experimental device monitored online by OCDR system

3 结果与讨论

飞秒激光加工参数众多,本实验系统中激光波长、脉冲宽度、聚焦物镜倍率和数值孔径为固定参数,利用聚焦透镜参数计算得到的激光焦斑^[43]直径为 496.75 nm ,焦深为 376.33 nm ,实际加工过程中仅通过改变激光脉冲能量、激光脉冲频率及直写速率来调控加工效果,下文将分别对其进行分析研究。

3.1 飞秒激光脉冲能量对加工光纤的影响

飞秒激光脉冲能量是引起材料性质改变的的决定性参数,本实验采用的单模光纤对飞秒激光通常是透明的,但经过物镜聚焦后激光峰值功率密度很容易达到石英材料的非线性效应阈值,引起强非线性吸收,从而诱导焦点处高度局域化的折射率改变^[20]。光纤中局部折射率改变则会引起光信号的反射现象,根据菲涅耳定律可知折射率改变量的大小与反射率正相关,这为 OCDR 在线监测提供了理论依据。

将待加工的光纤样品夹持在精心设计的 V 形槽光纤夹具上,利用三维超精密移动平台实现其精确的定位和移动,将光纤一端与 OCDR 系统连接,基于

飞秒激光在光纤纤芯中心位置写入点结构。为避免后加工的反射信号对先加工的反射信号测量的影响,采用从远端逐渐靠近 OCDR 测试端口的加工方式。图 4 所示为 OCDR 系统测得的反射率随飞秒激光脉冲能量变化的曲线,四条曲线标号 1~4 分别表示完全相同加工参数条件下重复四次实验所得的结果。实验过程中激光脉冲频率保持恒定,为 1 kHz ,仅改变脉冲能量。结果显示,随着脉冲能量的增加,根据反射率的变化规律,作用区域大致可分为图 4 中标号为 A、B、C 和 D 的 4 个作用区域,且 4 条曲线基本完全吻合,很好验证了实验的可重复性。其中: A 区未观测到任何反射信号,其原因是激光脉冲能量低于光纤非线性损伤阈值,此时光纤对激光透明;当激光能量达到 $\sim 0.355 \mu\text{J}$ 时(A 与 B 区交界点),观测到反射率突变现象,由此可确定激光能量的阈值点,且进入 B 区后,随着激光能量的增加反射率迅速增长,该区可作为飞秒激光光纤微结构加工的最佳工作区;当进入 C 区后,随着功率的进一步增加,反射率趋于稳定,可能原因是高斯光束束腰处的能量饱和且达到能量阈值;继续增加激光脉冲能量,进入

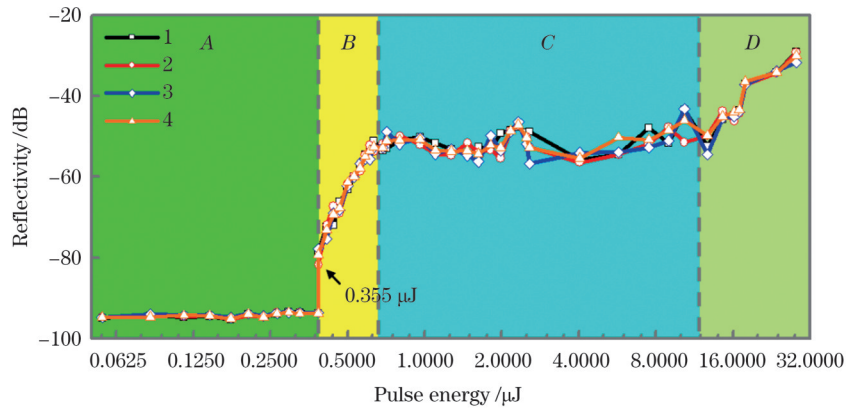


图4 OCDR测量的反射率随脉冲能量的变化

Fig. 4 Measured reflectivity by OCDR versus pulse energy

*D*区之后,反射率又开始快速增加,其原因为脉冲能量过高引起了孔洞效应^[44]。

为验证上述结论,本实验进一步分析了每个区域选取特征点的反射信号,并采用高倍显微镜对该位置形貌变化进行了表征。图5所示为OCDR测得的单点反射特性曲线,对应于显微图像中的左侧第一个点。值得注意的是:如果OCDR测量的多个结构在其分辨率范围内,则测得的反射曲线是多个结构反射叠加的结果;超出干涉长度,则反射率互不影响。由图5可知:*A*区域未测得反射信号,且显微图像上未观察到形貌变化;*B*、*C*和*D*区域测得的反射率逐渐增长,峰值反

射率分别为-66 dB、-51 dB和-35 dB。光纤的圆柱形结构对显微系统成像的影响使得微结构在显微图像上呈现长条形状。进一步分析发现,*D*区域出现了双峰现象。这是由于结构尺寸大于OCDR分辨率,且前后边缘存在折射率突变引起的强反射,也即产生了孔洞效应。图5还给出了光纤端面反射曲线,其峰值反射率约为-22 dB。上述结果表明,通过OCDR实测反射曲线能够精确灵敏地监测飞秒激光脉冲功率引起的材料性质改变,并且快速确定飞秒激光最优脉冲能量工作区(*B*区),在此区域调整脉冲能量可实现最大范围的材料改性控制。

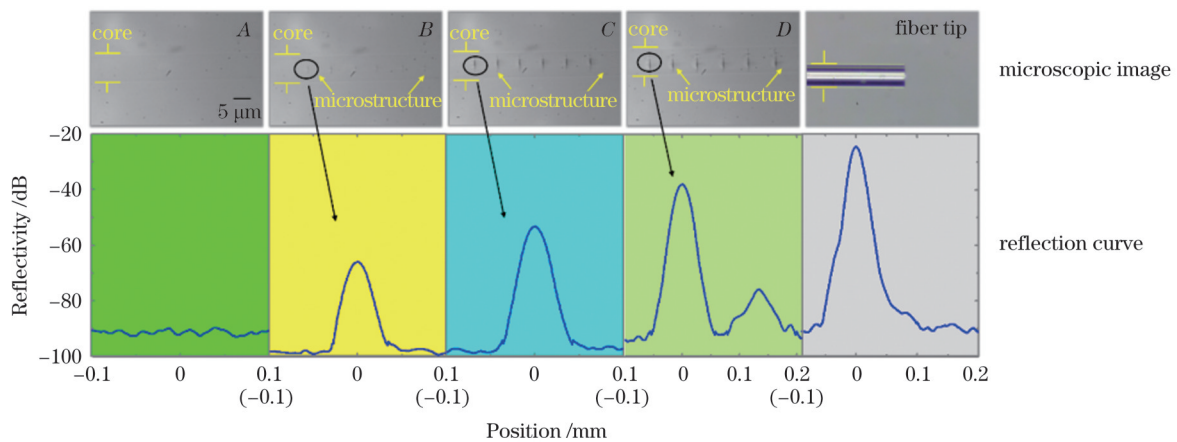


图5 不同脉冲能量区域特征点的OCDR测量反射曲线及显微图像

Fig. 5 Reflection curves and microscopic images of feature points in different pulse energy regions measured by OCDR

3.2 飞秒激光脉冲频率对加工光纤的影响

脉冲频率是影响飞秒激光直写微结构尺寸和形貌的关键参数之一。研究表明:随着飞秒激光频率的增加,脉冲产生的热量将发生累积,而折射率的改变涉及热效应的形成,因而加工尺寸增大^[45]。同样,光纤中折射率改变区域的面积增大也会引起反射率的增大,从而使得OCDR监测的反射曲线发生变化。

图6所示为OCDR系统测得的反射率随飞秒激光脉冲频率变化的曲线。实验过程中激光脉冲能量保持

恒定,为0.415 μJ ,仅改变脉冲频率。结果显示,随着脉冲频率的增加,根据反射率的变化规律,作用区域大致可分为图6中标号为*A*、*B*和*C*的三个作用区域。其中:*A*区域在低频时未观察到任何反射信号,说明此时光纤对激光透明;当激光的脉冲频率达到 ~ 50 Hz时(*A*与*B*区交界点),观察到反射率突变现象,且进入*B*区后,随着激光脉冲频率的增加反射率迅速增长,由此可确定激光脉冲频率的阈值点;在脉冲频率进入*C*区后,随着频率的进一步增加,反射率趋于稳定。考虑到脉冲能量和脉冲频率均存在阈值条件,本实验进一步

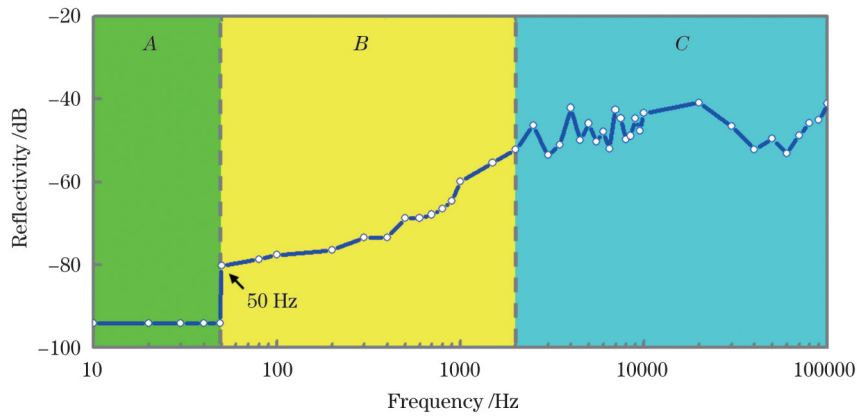


图 6 OCDR 测量反射率随脉冲频率变化

Fig. 6 Measured reflectivity by OCDR versus pulse frequency

在不同脉冲能量下扫描脉冲频率,得到的不同脉冲能量对应的脉冲频率的阈值条件如图 7 所示。结果显

示,随着脉冲能量的增加,飞秒激光脉冲的频率阈值点逐渐降低。

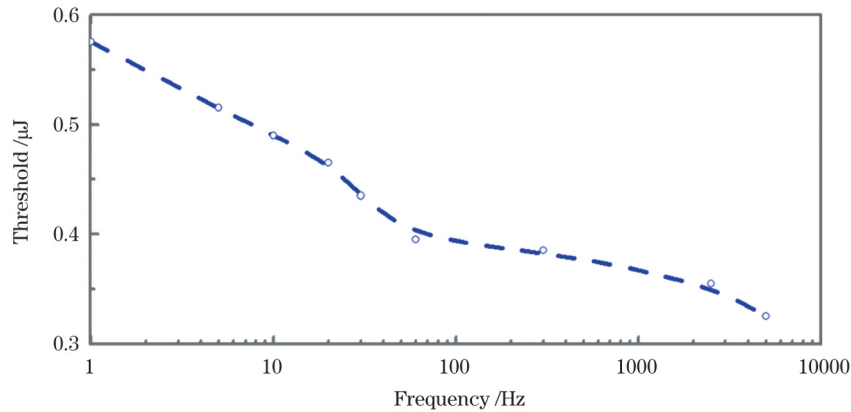


图 7 不同脉冲频率条件下的脉冲能量阈值变化

Fig. 7 Pulse energy threshold versus pulse frequency

3.3 飞秒激光直写速率以及扫描方式对加工光纤的影响

在飞秒激光工艺中,除了加工点外,还有线、面等多种结构,直写速率则是重要的影响因素。直写速率影响着相邻两光斑之间的能量累积效应,直接决定了一定尺度内的脉冲累积的数量,从而影响加工质量。速率越慢,脉冲数越多,能量累积越明显;而速率越快,脉冲数越少,能量积累越弱。

图 8 所示为 OCDR 系统测得的反射率随直写速率变化的曲线。实验过程中激光脉冲频率保持恒定,为 1 kHz,脉冲能量保持恒定,为 0.44 μJ ,仅改变直写速率。结果显示,随着直写速率的增加,其均匀性变差且反射率会逐渐变小,呈现反比关系。当直写速率为 10~20 $\mu\text{m/s}$ 时,反射率大小反映折射率改性程度,此时的加工均匀性最好。当直写速率为 300 $\mu\text{m/s}$ 时,未测得明显的反射。原因如下:由于激光直写速率直接影响相邻激光脉冲的叠加比例,当直写速率取最大值时,加工点间距越大,单位体积内的脉冲数目越小,飞秒激光加工接近于单脉冲加

工,此时反射率低于 OCDR 测量动态范围下限。此外,在直写区域首尾分别出现两个明显的反射峰,这是位移台步进电机启动和停止瞬间的暂态响应引起的。

针对脉冲能量高于损伤阈值但当直写速率为 300 $\mu\text{m/s}$ 时移动过程中未产生明显反射现象的情况,设计了重复扫描方案以确定该能量能够引起光纤折射率改性,扫描方向沿光纤纤芯传输方向,速度为 300 $\mu\text{m/s}$,扫描长度为 220 μm 。图 9 所示为 OCDR 监测得到的反射率随扫描次数变化的曲线,其中曲线标号 1~7 表示重复扫描直写次数。第一次扫描移动过程中 OCDR 未测得明显的反射,而逐渐增加扫描次数后,反射率逐渐增加并趋于稳定。由此确定该能量能够引起折射率改性。OCDR 没有测量到明显的反射,原因如下:高速直写加工导致单位体积内的脉冲数量过少,热累积微弱,进而改性区域的折射率变化和结构尺寸变化较小。上述分析表明,OCDR 不仅能实现静态加工参数的确定,而且具有对动态加工过程中的加工效果进行分布式监测的能力。

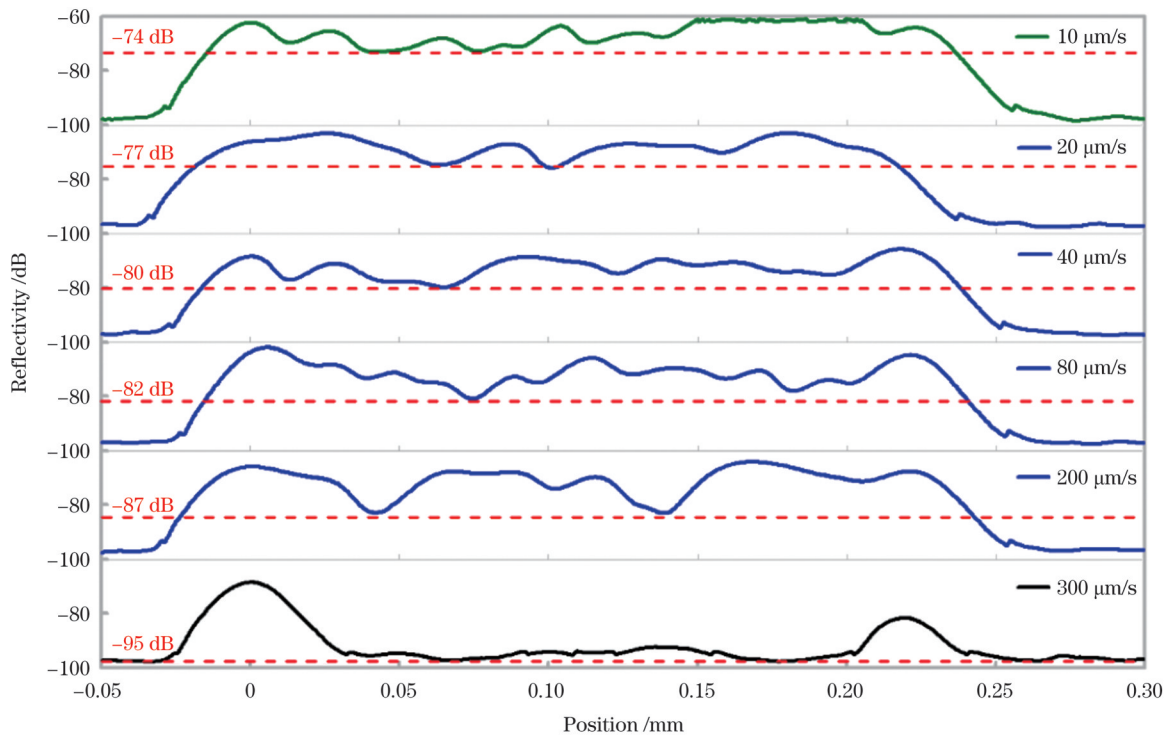
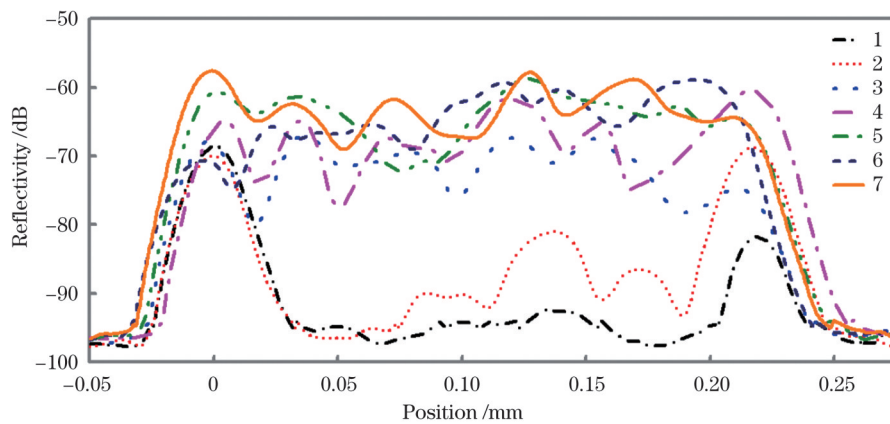


图8 OCDR测量反射曲线随直写速率变化

Fig. 8 Measured reflectivity by OCDR versus direct writing speed

图9 脉冲频率为1 kHz、脉冲能量为0.44 μJ 、直写速率为300 $\mu\text{m/s}$ 、扫描次数为7时的OCDR反射率变化Fig. 9 OCDR reflectivity changes when pulse frequency is 1 kHz, pulse energy is 0.44 μJ , direct writing speed is 300 $\mu\text{m/s}$, and number of scans is 7

4 结 论

高效的加工工艺参数监测手段可极大提升飞秒激光直写加工效率,降低工艺摸索成本。提出了一种基于高分辨率、高动态范围OCDR在线监测波导中飞秒激光直写微结构或器件的新技术。以飞秒激光直写光纤微结构为实验对象,研究了激光脉冲能量、脉冲频率及直写速率三个关键工艺参数对光纤反射特性的影响规律,建立了OCDR测量反射特征曲线与加工参数的对应关系。通过该模型能够快速准确地确定引起材料性质改变的激光能量和脉冲频率的阈值条件,且根据曲线变化趋势和反射峰特点可判断材料性质改变类型,为实际加工中快速选择最佳脉冲能量和脉冲频率提供

了参考。此外,利用OCDR的分布式、在线监测能力,还获得了直写速率对加工效果的影响规律。该技术为飞秒激光直写加工光波导微结构或器件工艺参数的快速确定及加工过程的实时监测提供了一种新的思路。

参 考 文 献

- [1] Momma C, Chichkov B N, Nolte S, et al. Short-pulse laser ablation of solid targets[J]. Optics Communications, 1996, 129(1/2): 134-142.
- [2] Antipov S, Ams M, Williams R J, et al. Direct infrared femtosecond laser inscription of chirped fiber Bragg gratings[J]. Optics Express, 2016, 24(1): 30-40.
- [3] Ioannou A, Theodosiou A, Caucheteur C, et al. Direct writing of plane-by-plane tilted fiber Bragg gratings using a femtosecond laser [J]. Optics Letters, 2017, 42(24): 5198-5201.
- [4] Kondo Y, Nouchi K, Mitsuyu T, et al. Fabrication of long-period

- fiber gratings by focused irradiation of infrared femtosecond laser pulses[J]. *Optics Letters*, 1999, 24(10): 646-648.
- [5] Li B Y, Jiang L, Wang S M, et al. Femtosecond laser fabrication of long period fiber gratings and applications in refractive index sensing[J]. *Optics & Laser Technology*, 2011, 43(8): 1420-1423.
- [6] Theodosiou A, Lacraz A, Polis M, et al. Modified fs-laser inscribed FBG array for rapid mode shape capture of free-free vibrating beams[J]. *IEEE Photonics Technology Letters*, 2016, 28(14): 1509-1512.
- [7] Yang K M, Liao C R, Liu S, et al. Optical fiber tag based on an encoded fiber Bragg grating fabricated by femtosecond laser[J]. *Journal of Lightwave Technology*, 2020, 38(6): 1474-1479.
- [8] Wei T, Han Y K, Tsai H L, et al. Miniaturized fiber inline Fabry-Perot interferometer fabricated with a femtosecond laser[J]. *Optics Letters*, 2008, 33(6): 536-538.
- [9] Ran Z L, Liu S, Liu Q, et al. Novel high-temperature fiber-optic pressure sensor based on etched PCF F-P interferometer micromachined by a 157-nm laser[J]. *IEEE Sensors Journal*, 2015, 15(7): 3955-3958.
- [10] Liu Y, Li M, Zhao P J, et al. High sensitive temperature sensor based on a polymer waveguide integrated in an optical fibre micro-cavity[J]. *Journal of Optics*, 2018, 20(1): 015801.
- [11] Deng J, Wang D N. Construction of cascaded Fabry-Perot interferometers by four in-fiber mirrors for high-temperature sensing[J]. *Optics Letters*, 2019, 44(5): 1289-1292.
- [12] Wang Q H, Zhang H, Wang D N. Cascaded multiple Fabry-Perot interferometers fabricated in no-core fiber with a waveguide for high-temperature sensing[J]. *Optics Letters*, 2019, 44(21): 5145-5148.
- [13] Dash J N, Cheng X, Gunawardena D S, et al. Rectangular single-mode polymer optical fiber for femtosecond laser inscription of FBGs[J]. *Photonics Research*, 2021, 9(10): 1931-1938.
- [14] Chen Q Q, Song H, Zhang F T, et al. A strategy for fabrication of controllable 3D pattern containing clusters and nanoparticles inside a solid material[J]. *Nanoscale*, 2017, 9(26): 9083-9088.
- [15] Grenier J R, Fernandes L A, Herman P R. Femtosecond laser writing of optical edge filters in fused silica optical waveguides[J]. *Optics Express*, 2013, 21(4): 4493-4502.
- [16] He Y, Zhu L, Liu Y, et al. Femtosecond laser direct writing of flexible all-reduced graphene oxide FET[J]. *IEEE Photonics Technology Letters*, 2016, 28(18): 1996-1999.
- [17] Wong S, Deubel M, Pérez-Willard F, et al. Direct laser writing of three-dimensional photonic crystals with a complete photonic bandgap in chalcogenide glasses[J]. *Advanced Materials*, 2006, 18(3): 265-269.
- [18] Yu F, Tian Z N, Piacentini S, et al. Resetting directional couplers for high-fidelity quantum photonic integrated chips[J]. *Optics Letters*, 2021, 46(20): 5181-5184.
- [19] Tan D Z, Wang Z, Xu B B, et al. Photonic circuits written by femtosecond laser in glass: improved fabrication and recent progress in photonic devices[J]. *Advanced Photonics*, 2021, 3(2): 024002.
- [20] Taylor R, Hnatovsky C, Simova E. Applications of femtosecond laser induced self-organized planar nanocracks inside fused silica glass[J]. *Laser & Photonics Review*, 2008, 2(1/2): 26-46.
- [21] Tu C H, Huang Z C, Zhang S G, et al. Second harmonic generation by femtosecond Yb-doped fiber laser source based on PPKTP waveguide fabricated by femtosecond laser direct writing[J]. *Optics Communications*, 2011, 284(1): 455-459.
- [22] Hirao K, Miura K. Writing waveguides and gratings in silica and related materials by a femtosecond laser[J]. *Journal of Non-Crystalline Solids*, 1998, 239(1/2/3): 91-95.
- [23] Ponader C W, Schroeder J F, Streltsov A M. Origin of the refractive-index increase in laser-written waveguides in glasses[J]. *Journal of Applied Physics*, 2008, 103(6): 063516.
- [24] Bricchi E, Klappauf B G, Kazansky P G. Form birefringence and negative index change created by femtosecond direct writing in transparent materials[J]. *Optics Letters*, 2004, 29(1): 119-121.
- [25] Liu X Q, Chen Q D, Guan K M, et al. Dry-etching-assisted femtosecond laser machining[J]. *Laser & Photonics Reviews*, 2017, 11(3): 1600115.
- [26] Li Z Z, Wang L, Fan H, et al. O-FIB: far-field-induced near-field breakdown for direct nanowriting in an atmospheric environment[J]. *Light: Science & Applications*, 2020, 9: 41.
- [27] Qian M D, Sun Y L, Hu Z Y, et al. Fluorescent chemo-sensors based on "dually smart" optical micro/nano-waveguides lithographically fabricated with AIE composite resins[J]. *Materials Horizons*, 2020, 7(7): 1782-1789.
- [28] Bruneau S, Hermann J, Dumitru G, et al. Ultra-fast laser ablation applied to deep-drilling of metals[J]. *Applied Surface Science*, 2005, 248(1/2/3/4): 299-303.
- [29] Coyne E, Magee J, Mannion P, et al. Study of femtosecond laser interaction with wafer-grade silicon[J]. *Proceedings of SPIE*, 2003, 4876: 487-499.
- [30] 赵强, 万辉, 于圣韬, 等. 飞秒激光制备柔性纳米多孔 Ag 材料的研究[J]. *中国激光*, 2021, 48(8): 0802009.
- Zhao Q, Wan H, Yu S T, et al. Investigation of flexible nanoporous silver materials fabricated by femtosecond laser[J]. *Chinese Journal of Lasers*, 2021, 48(8): 0802009.
- [31] Marshall G D, Dekker P, Ams M, et al. Directly written monolithic waveguide laser incorporating a distributed feedback waveguide-Bragg grating[J]. *Optics Letters*, 2008, 33(9): 956-958.
- [32] Döring S, Richter S, Nolte S, et al. *In situ* imaging of hole shape evolution in ultrashort pulse laser drilling[J]. *Optics Express*, 2010, 18(19): 20395-20400.
- [33] He J, He J, Xu X Z, et al. Single-mode helical Bragg grating waveguide created in a multimode coreless fiber by femtosecond laser direct writing[J]. *Photonics Research*, 2021, 9(10): 2052-2059.
- [34] Wang Y Y, Zhong L J, Chen Z, et al. Photonic lattice-like waveguides in glass directly written by femtosecond laser for on-chip mode conversion[J]. *Chinese Optics Letters*, 2022, 20(3): 031406.
- [35] Webster P J L, Muller M S, Fraser J M. High speed *in situ* depth profiling of ultrafast micromachining[J]. *Optics Express*, 2007, 15(23): 14967-14972.
- [36] Tomlins P H, Smith G N, Woolliams P D, et al. Femtosecond laser micro-inscription of optical coherence tomography resolution test artifacts[J]. *Biomedical Optics Express*, 2011, 2(5): 1319-1327.
- [37] Webster P J L, Wright L G, Mortimer K D, et al. Automatic real-time guidance of laser machining with inline coherent imaging[J]. *Journal of Laser Applications*, 2011, 23(2): 022001.
- [38] Hayashi N, Hoshikawa M, Ishii K, et al. In-process measurement of a keyhole using a low-coherence interferometer with a high repetition rate[J]. *Optics Express*, 2021, 29(20): 32169-32178.
- [39] Hasegawa S, Fujimoto M, Atsumi T, et al. In-process monitoring in laser grooving with line-shaped femtosecond pulses using optical coherence tomography[J]. *Light: Advanced Manufacturing*, 2022, 3(3): 33.
- [40] Takada K, Yokohama I, Chida K, et al. New measurement system for fault location in optical waveguide devices based on an interferometric technique[J]. *Applied Optics*, 1987, 26(9): 1603-1606.
- [41] Wu S B, Hao J X, Chen X J, et al. Location resolved internal structure identification and defect detection in PIC chips with optical coherence domain reflectometer[C]//Conference on Lasers and Electro-Optics: Applications and Technology, May 15-20, 2022, San Jose, California, USA. Washington, D. C.: Optica Publishing Group, 2022: JW3B.180.
- [42] 孟卓. 全光纤口腔 OCT 方法研究与系统研制[D]. 天津: 天津大学, 2008: 16-20.
- Meng Z. Research on method and system development of all fiber oral OCT[D]. Tianjin: Tianjin University, 2008: 16-20.
- [43] 国旗. 面向苛刻环境耐高温光纤光栅的制备及传感特性研究[D]. 长春: 吉林大学, 2022: 35-40.
- Guo Q. Research on fabrication and sensing characteristics of high temperature resistant fiber gratings for harsh environments[D]. Changchun: Jilin University, 2022: 35-40.

[44] Glezer E N, Mazur E. Ultrafast-laser driven micro-explosions in transparent materials[J]. Applied Physics Letters, 1997, 71(7): 882-884.

[45] Eaton S M, Zhang H B, Herman P R, et al. Heat accumulation effects in femtosecond laser-written waveguides with variable repetition rate[J]. Optics Express, 2005, 13(12): 4708-4716.

On-Line Monitoring of Optical Waveguide Micro-Structure Fabricated With Femtosecond Laser Direct Writing Based on OCDR

Xia Long^{1,2}, Wang Xinyue^{1,2}, Wu Shengbao^{1,2*}, Cui Shengwei^{1,2}, Feng Ting^{1,2}, Yao X. Steve^{1,2}

¹Photonics Information Innovation Center, College of Physics Science & Technology, Hebei University, Baoding 071002, Hebei, China;

²Hebei Provincial Center for Optical Sensing Innovations, Baoding 071002, Hebei, China

Abstract

Objective Femtosecond laser direct-writing plays a key role in optical waveguide device fabrication owing to its advantages of being maskless, true three-dimension, high precision, and flexibility. However, due to the lack of a mature theoretical model that can completely describe the interaction mechanism of the laser pulse with different materials, numerous experiments are required to determine the set of optimal processing parameters. Scanning electron microscopy or atomic force microscopy can provide high-resolution images of fabricated samples, but they generally need the sample to be destroyed, which is a time-consuming process. An optical microscope combined with a laser processing system can be used for in-process monitoring. However, the material to be processed needs to be transparent to illumination, and the resolution of the optical microscope is generally limited. Recently, methods based on optical coherence imaging have been proposed to obtain depth information in addition to a two-dimensional image. However, owing to the limited dynamic range detection, these methods cannot be used to measure the weak scattered signal induced by the small refractive index of the material in optical waveguide device processing. Therefore, in-process techniques for efficiently determining the processing parameters of femtosecond laser direct-writing optical waveguide devices are useful and significant.

Methods The backward reflection signal induced by femtosecond laser direct-writing optical waveguide devices was used for the in-process monitoring of the key processing parameters. We developed coherence domain reflectometry (OCDR) (Fig. 1) with a large reflection dynamic range (-10 dB to -95 dB) and high accuracy (± 1.0 dB) to measure the reflection signal. By directly writing micro-nano defects in the core of a single-mode optical fiber with different processing parameters, backward reflection signals were generated and subsequently detected by the OCDR connected to one port of the fiber (Fig. 2). The variation tendency of the measured reflection curve was used to determine the optimal processing parameters, and the reflection for a specific case was used to identify the type of change in the material (Fig. 5).

Results and Discussions The influence of three key parameters, that is, the pulse energy, pulse frequency, and direct writing speed of the femtosecond laser, on the backward reflection signal in fiber micro-nano processing is studied using OCDR. By increasing the pulse energy (fixed pulse frequency of 1 kHz), the variation tendency of the measured reflectivity can be divided into four different regions *A*, *B*, *C*, and *D* (Fig. 4), where the abrupt change point ($0.355 \mu\text{J}$) between *A* and *B* is identified as the pulse energy threshold, and *B* is the optimal region for optical waveguide device writing owing to its relatively low return loss and large reflectivity tuning range. A similar behavior is also observed when the pulse frequency is changed (fixed pulse energy $0.415 \mu\text{J}$) (Fig. 6). By scanning the pulse frequency at different pulse energies, the threshold points for different setups of the two key parameters are obtained (Fig. 7). The results show that the threshold energy gradually decreases with an increase in the pulse frequency. By the distributed monitoring of the reflection signal along the direct writing path, we find that the reflectivity decreases with an increase in the writing speed (Fig. 8), and the uniformity of the reflectivity curve can be improved by multiple writing (Fig. 9).

Conclusions A distributed sensing technique based on OCDR for the in-process monitoring of direct-writing microstructures in optical waveguides with femtosecond pulses is proposed. The measured backward reflection signal is used to determine the optimal fabrication parameters. The influence of three key parameters, that is, pulse energy, pulse frequency, and direct writing speed, on the backward reflection signal in fiber micro-nano processing is studied by OCDR. The measured results show that the threshold conditions of the pulse energy and pulse frequency that cause material property changes can be determined quickly and accurately via abrupt changes in the reflection curve, and the type of material property change can also be identified according to the curve variation and reflectivity. In addition, the influence of the direct writing speed on the fabrication uniformity is determined by taking advantage of the distributed sensing ability of the OCDR. This work provides a non-destructive, efficient, and in-process solution for exploring the processing parameters of femtosecond laser direct-writing optical waveguide devices.

Key words laser technique; femtosecond laser; optical waveguide; micro-nano processing; distributed fiber sensing; reflection characteristics